Acta Biomaterialia 65 (2018) 259–271

Contents lists available at ScienceDirect

Acta Biomaterialia

journal homepage: www.elsevier.com/locate/actabiomat

Full length article

Monomer sequence in PLGA microparticles: Effects on acidic microclimates and *in vivo* inflammatory response

Michael A. Washington [a], Stephen C. Balmert [d,g], Morgan V. Fedorchak [b,c,g,h], Steven R. Little [b,c,d,e,f,g], Simon C. Watkins [i,j], Tara Y. Meyer [a,g,*]

[a] Department of Chemistry, University of Pittsburgh, Pittsburgh, PA 15260, USA
[b] Department of Chemical and Petroleum Engineering, University of Pittsburgh, Pittsburgh, PA 15260, USA
[c] Department of Ophthalmology, University of Pittsburgh, Pittsburgh, PA 15260, USA
[d] Department of Bioengineering, University of Pittsburgh, Pittsburgh, PA 15260, USA
[e] Department of Immunology, University of Pittsburgh, Pittsburgh, PA 15260, USA
[f] Department of Pharmaceutical Sciences, University of Pittsburgh, Pittsburgh, PA 15260, USA
[g] McGowan Institute for Regenerative Medicine, University of Pittsburgh, Pittsburgh, PA 15260, USA
[h] Fox Center for Vision Restoration, University of Pittsburgh, Pittsburgh, PA 15260, USA
[i] Department of Cell Biology, University of Pittsburgh, Pittsburgh, PA 15260, USA
[j] Center for Biologic Imaging, University of Pittsburgh, Pittsburgh, PA 15260, USA

ARTICLE INFO

Article history:
Received 20 April 2017
Received in revised form 24 October 2017
Accepted 30 October 2017
Available online 31 October 2017

Keywords:
Poly(lactic-*co*-glycolic acid)
Two-photon microscopy
Acidic microclimate
Foreign body response
Sequenced copolymers

ABSTRACT

Controlling the backbone architecture of poly(lactic-*co*-glycolic acid)s (PLGAs) is demonstrated to have a strong influence on the production and release of acidic degradation by-products in microparticle matrices. Previous efforts for controlling the internal and external accumulation of acidity for PLGA microparticles have focused on the addition of excipients including neutralization and anti-inflammatory agents. In this report, we utilize a sequence-control strategy to tailor the microstructure of PLGA. The internal acidic microclimate distributions within sequence-defined and random PLGA microparticles were monitored *in vitro* using a non-invasive ratiometric two-photon microscopy (TPM) methodology. Sequence-defined PLGAs were found to have minimal changes in pH distribution and lower amounts of percolating acidic by-products. A parallel scanning electron microscopy study further linked external morphological events to internal degradation-induced structural changes. The properties of the sequenced and random copolymers characterized *in vitro* translated to differences in *in vivo* behavior. The sequence alternating copolymer, poly LG, had lower granulomatous foreign-body reactions compared to random racemic PLGA with a 50:50 ratio of lactic to glycolic acid.

Statement of Significance

This paper demonstrates that changing the monomer sequence in poly(lactic-*co*-glycolic acid)s (PLGAs) leads to dramatic differences in the rate of degradation and the internal acidic microclimate of microparticles degrading *in vitro*. We note that the acidic microclimates within these particles were imaged for the first time with two-photon microscopy, which gives an extremely clear and detailed picture of the degradation process. Importantly, we also document that the observed sequence-controlled *in vitro* processes translate into differences in the *in vivo* behavior of polymers which have the same L to G composition but differing microstructures. These data, placed in the context of our prior studies on swelling, erosion, and MW loss (*Biomaterials* **2017**, *117*, 66 and other references cited within the manuscript), provide significant insight not only about sequence effects in PLGAs but into the underlying mechanisms of PLGA degradation in general.

© 2017 Acta Materialia Inc. Published by Elsevier Ltd. All rights reserved.

* Corresponding author at: Department of Chemistry, University of Pittsburgh, 219 Parkman Avenue, Pittsburgh, PA 15260, USA.
E-mail address: tmeyer@pitt.edu (T.Y. Meyer).

https://doi.org/10.1016/j.actbio.2017.10.043
1742-7061/© 2017 Acta Materialia Inc. Published by Elsevier Ltd. All rights reserved.

1. Introduction

The favorable hydrolytic degradation profiles and biocompatibility of poly(lactic-*co*-glycolic acid)s (PLGAs) have resulted in extensive research into their application as components in drug delivery systems (DDSs) [1,2]. The performance of DDSs made from PLGAs have been linked in these studies to several characteristics including ester hydrolysis rates, diffusion, swelling, erosion, and local pH drop [3–6]. Although these processes can be partially tuned by varying the L:G-ratio and molecular weight of the random copolymer, the lack of fine control over the properties may contribute to the surprisingly low commercial use of PLGAs [7]. Despite thousands of literature reports on PLGA DDSs, relatively few PLGA-based products have garnered FDA and EMA approval over the past three decades [8]. This limited degree of translation suggests that there is a clear unmet need for alternative methods that optimize the performance of PLGA matrices.

We have recently reported that precise control over monomer sequence can be utilized to tune *in vitro* PLGA degradation behavior for various PLGA matrices. In Li et al., for example, we describe the sequence-dependent degradation behavior of microparticles, demonstrating that thermal properties, molecular weight loss, lactic acid release, and rhodamine B release rates were dramatically different for random PLGAs vs. sequenced PLGAs prepared with the same L:G-ratio and molecular weights [9,10]. Specifically, we found that *in vitro* degradation and release rates were slower and more gradual for microparticles prepared with periodic sequences, e.g., $(LG)_n$, $(LLG)_n$ relative to random analogues. More recently, in Washington et al., we demonstrated that compression-molded implants fabricated with sequenced PLGAs exhibited minimal *in vitro* changes in swelling, delayed onsets of erosion, and more gradual changes in molecular weight and dispersity compared to random PLGAs with the same overall compositions [11]. Finally, in both of these studies, we were able to show that by varying the structural and/or stereosequence that the degradation-related properties could be tuned. We note that there are a number of recent reports concerning both the development of new general synthetic strategies for creating sequenced copolymers as well as studies correlating sequence with properties [12–20].

Significant precedent for our strategy of controlling sequence can also be found in studies on random poly(α-hydroxy acid)s in which properties are mapped to changes in the statistical distributions of monomers. For instance, Abe and Tabata have demonstrated that the thermal properties and crystalline structures for a class of periodic aliphatic polyesters may be varied over a wide range of temperatures based on stereosequence manipulations [21,22]. Sarasua and coworkers have further linked statistical variations in chain microstructure to various hydrolytic degradation rates in poly(lactide-*co*-ε-caprolactone) matrices [23–28]. Finally, Albertsson and coworkers, determined that the distribution of hydrolytically-accessible 1,5-dioxepan-2-one linkages had a profound effect on the release rates of acidic degradation products in triblock, multiblock, and random crosslinked caprolactone/1,5-dioxepan-2-one copolymers [29].

This study adds to our previous work on sequenced PLGAs, specifically on the characterization of how sequence affects the accumulation, distribution, and release of acidic by-products during PLGA degradation. These by-products represent a significant challenge to using poly(α-hydroxy acid)s in applications because acid can degrade macromolecular payloads that have been encapsulated in PLGA matrices and can lead to local inflammation when implanted *in vivo* [30]. Previous attempts to address this issue have typically involved the addition of neutralizing agents and other excipients to control the internal acidic microclimate pH (μpH) [31] and/or the incorporation of anti-inflammatory agents such as dexamethasone and tripolyphosphate to minimize the impact of acidity on tissues near the injection site [32–34]. Although these methods have proven effective in specific studies, the addition of external agents necessarily introduces new factors that can affect the drug release kinetics, immune response, and degradation profile of the PLGA matrix. Based on our reported observation that lactic acid release rates were greatly suppressed in sequenced copolymers relative to random PLGAs [9], we hypothesize that sequence can be used as a tool to control the acidic microclimate within a polymer microparticle and acid-induced inflammation of DDSs. This approach is particularly attractive since the potential complications that could arise from the incorporation of additives can be avoided.

To understand how sequence affects acidity within a PLGA microparticle, we characterized the *in vitro* spatial distribution of low pH regions in PLGA as a function of sequence and stereosequence using a non-invasive ratiometric two-photon microscopy (TPM) method. Other non-invasive efforts to visualize the pH within random PLGA microparticles have been previously reported and include electron paramagnetic resonance spectroscopy (EPR) [35–38] and confocal laser scanning microscopy (CLSM) [30,39–44]. Although EPR methods demonstrated that the internal pH of PLGA particles can be as low as pH = 2, CLSM studies, conducted on particles loaded with pH-sensitive dyes, make it possible to spatially map the pH within small particles. Using CLSM methods, Langer and Schwendeman independently reported an internal pH range within microparticles composed of random PLGAs of 1.5–3.5 after 15 d and 3.2–3.4 after 28 d of *in vitro* hydrolytic degradation, respectively. Moreover, Schwendeman and coworkers extensively studied how L:G-ratio, molecular weight, microparticle size, and emulsion method (W/O/W and O/O) influenced μpH kinetics and determined that L:G-ratio and molecular weight contributed to differences in μpH distribution and kinetics. Random PLGA with an L:G-ratio of 50:50 and low molecular weight were also found to exhibit earlier onsets of acid accumulation, lower acidic distribution after 28 d, and notable changes in morphology. Degradation-induced morphological changes were also observed by Langer and coworkers using scanning electron microscopy (SEM); increasing surface pores and slight plasticization for 50:50 L:G-ratio PLGA microparticles were observed [30]. We note that we have also previously utilized CLSM to map the drug distribution a dextran-labeled Texas Red dye [45]. Other strategies for measuring the acidity of PLGA, aside from the aforementioned non-invasive methods have been reported and include indirect pH measurements of the incubation media potentiometric measurements recorded using inserted pH probes [37,46–48].

In the current study, we focused upon the difference in pH distribution within microparticles as a function of monomer sequence using two-photon microscopy (TPM). We and others have demonstrated the TPM offers distinct advantages over confocal microscopy for monitoring ratiometric probes within cells and other structures including minimization of data-destroying photobleaching and the ability to image at greater depths [49–52]. Finally, as we are also interested in understanding whether sequence-based differences in pH distribution within microparticles translate into differences in *in vivo* performance we also report herein a comparison of the inflammatory response to implanted sequenced and random copolymer microparticles.

2. Materials and methods

2.1. Materials

Poly(D,L-lactide-*co*-glycolide) with a copolymer ratio of 50:50 and 65:35 were purchased from Durect Corporation (Birmingham,

AL). Poly(L-lactide-*co*-glycolide) with a 50:50 L:G-ratio was purchased from Changchun SinoBiomaterials Co. Ltd. (Changchun, China). The pH sensitive fluorescent probe, LysoSensor™ Yellow/Blue DND-160 (PDMPO) (MW 366.42), was purchased from Life Technologies (Eugene, OR, USA) as a 1 mM solution in dimethylsulfoxide (DMSO). Polyvinyl alcohol (PVA, MW 25 kDa, 98% hydrolyzed) was from Polysciences (Warrington, PA). Sequence PLGA copolymers were prepared using previously reported methods [53].

2.2. Characterization

Molecular weights and dispersities were acquired on a Waters GPC system (tetrahydrofuran (THF), 0.5 mL/min) with Jordi 500 Å, 1000 Å, and 10,000 Å divinylbenzene (DVB) columns and refractive index detector (Waters), which was calibrated relative to polystyrene standards. Thermal properties of all polymers prior to and after single-emulsion (O/W) microparticle preparation were obtained using TA Instruments Q200 DSC. Data were collected with a heating and cooling rate of 10 °C/min. The glass transition temperatures (T_g) for polymers as synthesized were collected during the second heating cycle while the O/W microparticles were collected in the first heating cycle. The glass transition temperatures are reported as the half-step Cp extrapolated. The ^{1}H and ^{13}C NMR spectra were obtained in $CDCl_3$ using a 500 MHz Bruker Avance III spectrometer at 293 K and calibrated to the residual solvent peak at δ 7.26 ppm (^{1}H) and δ 77.00 ppm (^{13}C).

2.3. Preparation of PLGA microparticles

PLGA microparticles containing the pH sensitive dye, LysoSensor™ Yellow/Blue DND-160 (PDMPO) were synthesized using a single-emulsion process [1,54]. Briefly, under low light conditions, PLGA (300 mg) was dissolved in dichloromethane (4 mL) followed by the addition of 200 μL of 1.0 mM LysoSensor™ in DMSO and the mixture was vortexed 1 min. The solution was added dropwise through a 250 μm sieve (U.S. Standard sieve series; ASTM E-11 specifications; Dual MFG Co.; Chicago, IL) into a 1% w/v (aq) PVA solution stirred at 600 RPM for 3 h at 23 °C. The resulting microspheres were centrifuged at 4 °C, 1000 RPM, 8 min and washed with deionized (DI) water (4×). The microspheres were briefly re-suspended in deionized water (5 mL), flash frozen with liquid nitrogen and lyophilized for 3 d (VirTis Benchtop K freeze dryer, Gardiner, NY; operating at 100 mTorr). For the control, unloaded microparticles, the procedure described above was used while omitting the addition of the pH sensitive dye.

2.4. Standard curve of fluorescent intensity ratio vs. pH

Buffers of pH 2.8 to 6.4 were prepared using 0.1 M citric acid and 0.2 M Na_2HPO_4 solutions. An aliquot of LysoSensor™ Yellow/Blue DND-160 was added to the buffer solutions yielding a concentration of 2.0 μM. A Varian Cary Eclipse Fluorescence Spectrophotometer coupled to a personal computer with software (cary eclipse software) provided by Varian was utilized to monitor the emission spectra of the pH probe as a function of pH. The standard dye solutions were excited at the isosbestic point λ = 360 nm and the fluorescence spectra were recorded from 375 to 700 nm. The standard curve was established by plotting the ratio of the fluorescent intensities at two emission wavelengths, 450 nm and 530 nm, versus the pH of that solution. Under these conditions, error in pH was estimated as ±0.5 for any single measurement.

2.5. Microclimate pH mapping inside microparticles

PLGA microparticles (40–41 mg) were incubated in 2.00 mL of phosphate buffer saline (10.0 mM, pH = 7.4) at 37 °C under continuous rotation at 8 rpm (Labquake Tube Rotator, Thermo Scientific). At specific time points, a 100 μL aliquot was deposited on a glass microscope slide and imaged using a two-photon microscope system. Fresh buffer was added to maintain the initial sample volume of 2.00 mL.

2.6. Two photon microscopy imaging

Two-photon images of sequenced and random PLGAs were captured using an Olympus FV1000MPE multiphoton scanning microscope (Olympus Corporation; Tokyo, Japan). The TPM system was configured with a mode-locked Ti:Sapphire laser (Chameleon Vision; Coherent; Santa Clara, CA) set to 740 nm, 5.4% intensity and a Olympus upright optical microscope with a 25×, XL Plan N 1.05 N.A. water immersion objective lens (Olympus). The multiphoton emission of the LysoSensor™ DND-160 pH probe at near neutral and acidic pH was captured using 420–460 nm (near neutral pH) and 500–550 nm (acidic pH) emission filters. FLUOVIEW Ver. 2.1c software (Olympus) was utilized to acquire multiple XY scans (508× 508 μm; 0.503 μm/pixel resolution; 12.5 μsec/pixel) in 1.5 μm increments in the Z-direction. TPM images of each microparticle formulation were acquired in multiple regions (n = 4).

2.7. Image processing for pH distributions

TPM images were processed using Nikon-Elements AR 4.50 software package. A threshold was applied to each channel with a 3× smoothing algorithm. The pH vs. I_{450nm}/I_{530nm} titration curve was applied images containing 8–10 microparticles and the corresponding pixel intensity ratio frequency vs. pH histograms were constructed. The histograms were processed using OriginPro 2016 where a LOWESS smoothing algorithm was applied to remove the high-frequency components. Based on the number of replicates and error associated with the ratiometric calculation method (pH ± 0.5) for determining pH, the corresponding values within the pH distribution profiles are estimated to have an accuracy of pH ± 0.2.

2.8. SEM characterization of microparticles over time

Five samples of microparticles for each PLGA (10 mg) were incubated in 1.00 mL of phosphate buffer saline (10.0 mM, pH = 7.4; Gibco by Life Technologies) at 37 °C under continuous rotation at 8 rpm (Labquake Tube Rotator, Thermo Scientific). This study was run in parallel with the two-photon study. At specific time points, week(s) 1, 2, 3, 4 and 5, the microparticles were flash frozen with liquid nitrogen and lyophilized for 3 d prior to imaging. The structural integrity and surface morphology of sequenced and random PLGAs during degradation were characterized using the JSM-6510LV SEM system. The lyophilized microparticles were sputtered with palladium under an argon atmosphere for 2 cycles of 2.5 min, 30 mA, with a Cressington Sputter Coater 108auto (Ladd Research, Williston, VT). The images were captured under high vacuum at an acceleration voltage of 2.5–5 kV with the stage titled 5°. Three images from separate regions of the sample were captured under various magnifications of ×150, ×350, and ×800.

2.9. In vivo studies and histology

Female C57BL/6J wild-type mice were purchased from The Jackson Laboratory (Bar Harbor, ME) and used at 8–12 weeks of age. All mice were maintained under specific pathogen-free conditions at the University of Pittsburgh, and experiments were conducted with the approval of the Institutional Animal Care and Use Committee and in accordance with NIH guidelines. Mice were subcutaneously injected in the scruff with PLGA microspheres (15 mg)

suspended in sterile phosphate buffered saline. Mice were euthanized at 2 weeks and 4 weeks ($n = 2$ mice per group per time point). Tissues at the injection sites were excised, flash frozen fresh, and cryosectioned. Sections were stained with hematoxylin and eosin (H&E), and imaged using a Nikon Eclipse E400 microscope.

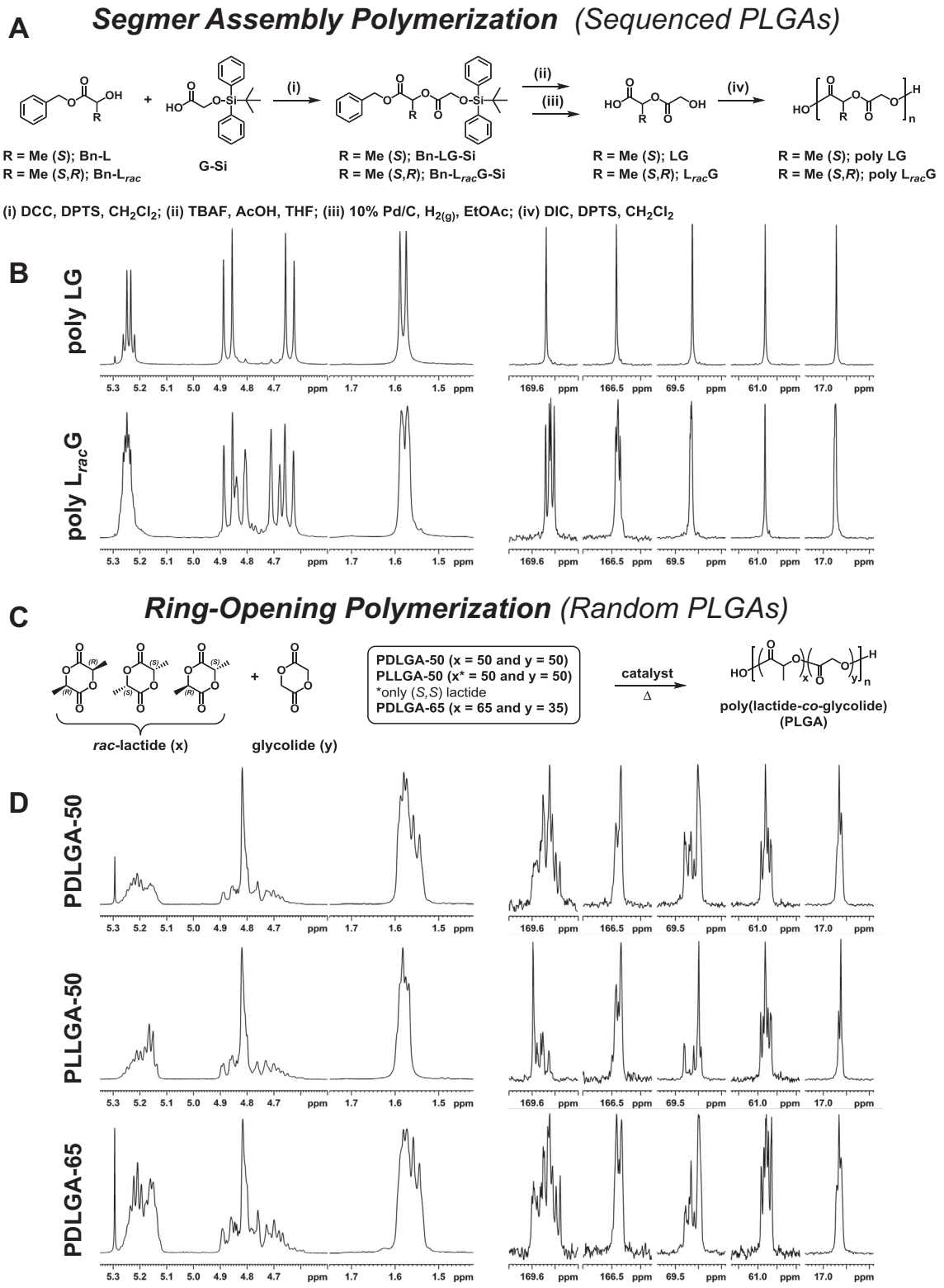

Fig. 1. Synthetic preparation of sequenced and random PLGAs and NMR characterization (A) Synthesis of sequenced PLGA copolymers via segmer assembly polymerization (SAP) methodology. (B) ^{1}H NMR spectra (left) and ^{13}C NMR spectra (right) for the sequenced periodic PLGA copolymers. (C) Ring-opening polymerization synthesis of the purchased random PLGAs. (D) ^{1}H NMR spectra (left) and ^{13}C NMR spectra (right) for the random PLGA copolymers. For all polymers, the ^{1}H NMR spectra display the methine, methylene, and methyl resonances from left to right. ^{13}C NMR spectra display the resonances for glycolyl, lactidyl, methine, methylene, and methyl carbons from left to right.

3. Results

3.1. PLGA copolymer and microparticle synthesis and characterization

The sequenced periodic copolymers **poly LG** and **poly $L_{rac}G$** were prepared as described previously using segmer assembly polymerization (SAP) (Fig. 1A) [53]. It is important to note that the synthetic method has been optimized to produce copolymers with a very high degree of sequence fidelity [55]. The naming convention for these polymers includes the description of the exact sequence of monomers in a segmer unit wherein the L-lactic acid unit, *rac*-lactic acid unit, and glycolic acid units are abbreviated as L, L_{rac}, and G, respectively. The purchased random copolymers were prepared by ring-opening polymerization (ROP, Fig. 1C). **PDLGA-50** is racemic variant of the random copolymer with and L:G-ratio of 1:1 while **PLLGA-50** is the stereopure analogue. **PDLGA-65** is racemic but has a 2:1 L:G-composition. The molecular weights of sequenced PLGAs prepared by SAP and purchased random PLGA controls were comparable, 21–30 kDa (Table 1, Fig. S1).

Microparticles, both with and without the inclusion of the pH-sensitive dye LysoSensor™ Yellow/Blue DND-160, were prepared by a single-emulsion method. The T_gs for all polymers were between 47 and 50 °C as synthesized but decreased by 2–6 °C after formulation into microparticles (Table 1, Fig. S2). The surface morphology of the non-dye loaded microparticle controls was characterized using scanning electron microscopy (Fig. S3). The microparticles exhibited some dispersity with sizes ranging from 50 to 150 μm.

The sequence and stereopurity of the periodic PLGA copolymers were confirmed using ^{1}H and ^{13}C NMR (Fig. 1B and D). We have shown previously through extensive studies that the NMR spectra of sequenced PLGAs is extraordinarily sensitive to sequence with the result that we can *unambiguously* assign the sequence of any polymer by comparison to authentic samples and can determine if a particular sample is contaminated with other sequence errors [53,55]. Particularly sensitive are the chemical shifts of the diastereotopic glycolic methylene peaks that exhibit significant differences that correlate with the relative stereochemistry of nearby lactic units. It can be seen, for example, in Fig. 1B that there is one major pair of doublets associated for the glycolic units of the stereopure **poly LG** while multiple peaks appear in that same regions for **poly $L_{rac}G$**, corresponding to stereoisomers that have been previously shown to correlate to a tetrad-level of resolution, e.g. *iss* vs. *iis* [53,56]. On that basis, the weak peaks visible in the glycolic region of the **poly LG** can be attributed to a small amount (<5%) of epimerization. Similar analyses can be made for the ^{13}C NMR spectra, with the carbonyl resonances being the easiest to interpret.

As we will be exploring the degradation behavior of these sequenced copolymers it is important to note that we have previously exploited the sensitivity of these NMR spectra to sequence to verify that sequence scrambling does not occur to a significant extent during hydrolytic degradation [11,53].

3.2. LysoSensor™ yellow/blue DND-160 pH-dependent fluorescent response

LysoSensor™ Yellow/Blue DND-160 (PDMPO) was used to measure the internal pH of PLGA microspheres. Within a working pH range of 6.4–2.8, the emission intensity of this molecular probe

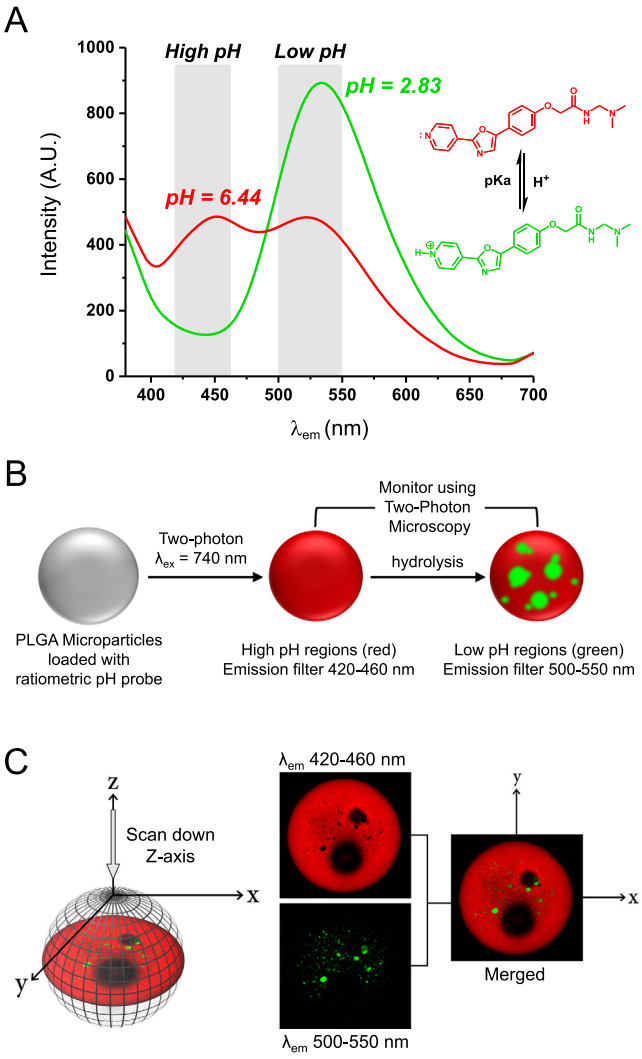

Fig. 2. Ratiometric properties of pH-sensitive dye, two-photon microscopy experimental overview, and image acquisition parameters. (A) Chemical structure, emission profiles (λ_{ex} = 360 nm), and emission window regions for the deprotonated and protonated LysoSensor™ pH probe. (B) The low energy two-photon excitation, λ_{ex} = 740 nm ≈ 2× one-photon λ_{ex}, penetrates deep into the interior of the microparticles providing a detailed pH map (C) Z-stack image acquisition of microparticles in solution were monitored using two separate λ_{em} windows. Merged images are displayed throughout the manuscript.

Table 1
Characterization data for sequenced and random PLGAs.

Polymer	M_n [a] (kDa)	M_w [a] (kDa)	Đ [a]	T_g [b] (°C)	T_g [c] (°C)	L:G ratio [d]	Control yield (%)	Dye-loaded yield (%)
Poly LG	21.4	32.1	1.5	50	48	50:50	47.1	57.7
Poly $L_{rac}G$	29.7	43.9	1.5	49	45	50:50	61.3	62.0
PDLGA-50	28.9	38.2	1.3	48	42	51:49	60.8	61.7
PLLGA-50	22.4	31.4	1.4	47	44	54:46	65.4	60.2
PDLGA-65	28.5	38.3	1.3	48	45	65:35	64.2	57.3

[a] Molecular weights determined using THF size exclusion chromatography relative to polystyrene standards.
[b] Standard glass transition temperatures were measured in the second heating cycle (10 °C/min, half C_p extrapolated).
[c] Glass transition temperatures of microparticles after single emulsion preparation were measured in the first heating cycle (10 °C/min, half C_p extrapolated).
[d] Ratio of lactic (L) and glycolic (G) units was determined using ^{1}H NMR spectroscopy.

shifts from $\lambda_{max} \sim 450$ nm to $\lambda_{max} \sim 530$ nm with acidifying pH (Fig. 2A). A series of citric acid: sodium phosphate dibasic pH buffer solutions were utilized to construct a pH vs. I_{450nm}/I_{530nm} standard curve used for interpretation of the TPM data (Figs. S4 and S5). Briefly, pH buffer solutions of pH 2.83–6.44 with 2 μM dye concentrations were excited at the isosbestic point λ_{ex} 360 nm and their ratiometric response intensity was determined. Using a third-order polynomial function ($r^2 = 0.994$), the optimal pH detection range was determined to be between pH 3.4 and 5.8 with the regions of pH 2.8–3.4 and pH 5.8–6.4 being slightly outside the detection range. Previous reports have verified that the ratiometric emission properties are independent of concentrations above 1 μM [40,44]. Microparticles were loaded by exposure to a 50 μM solution of the LysoSensor™ dye during single-emulsion fabrication. Quantitative loading efficiencies were not determined in this study. Instead, the loading efficiency was qualitatively determined by the presence of emission bands associated with the dye. We had previously reported that **poly LG** and **poly L_{rac}G** exhibited a lower loading efficiency that the random analogue [9] and the same qualitative behavior was observed for the LysoSensor™ dye in this investigation.

3.3. Internal acidity and morphology changes within sequenced and random PLGA microparticles

The effect of monomer sequence on the evolution and distribution of acidity within PLGA microparticles was investigated using two-photon microscopy (Fig. 2B). The pH probe, LysoSensor™, was loaded into 50–150 μm microparticles using a single-emulsion method. At various time points over 8 weeks, internal slices of aqueous microparticle suspensions were imaged at various depths. The ratiometric pH response was captured using a V/G multiphoton emission filter set, translating to red (near neutral pH) and green (acidic pH) signals (Fig. 2C). The pH distribution studies for sequenced PLGAs, was limited to 3 weeks due to low dye loading and long-term dye leaching. The random 50:50 analogues were monitored over 2 weeks while minimal dye leaching for **PDLGA-65** allowed the pH to be monitored over 8 weeks. Representative images of microparticles over a 2-week time period are shown in Fig. 3. Additional data for **poly L_{rac}G**, **poly LG**, and **PDLGA-65** at later time points can be found in Fig. 4. High resolution TPM images of single microparticles displaying characteristic acidic microclimate features are included for reference in Fig. S6. As we

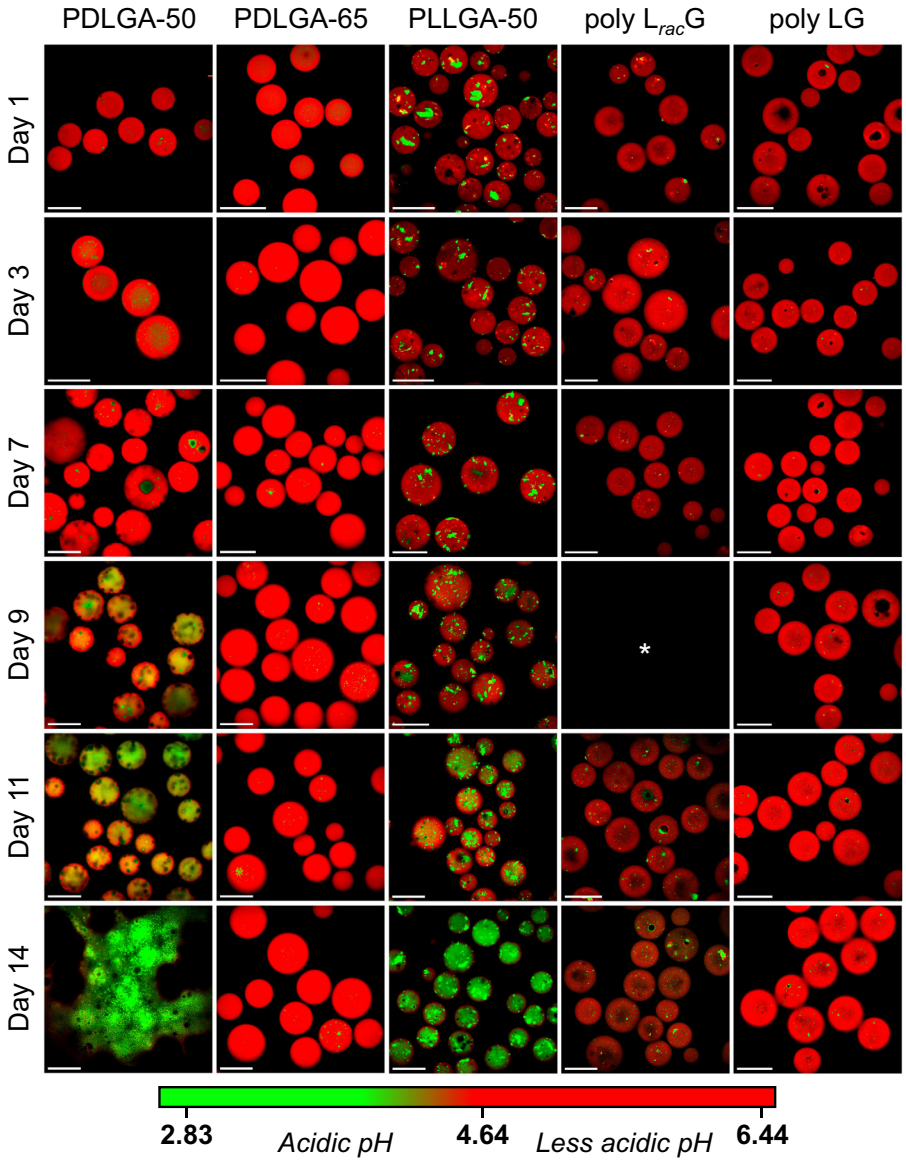

Fig. 3. Internal acidic microclimate distributions of sequenced and random PLGA copolymers after 1, 3, 7, 9, 11 and 14 d *in vitro* (brightness normalized). *Image not obtained due to laser mode-locking complications. Scale bar = 100 μm.

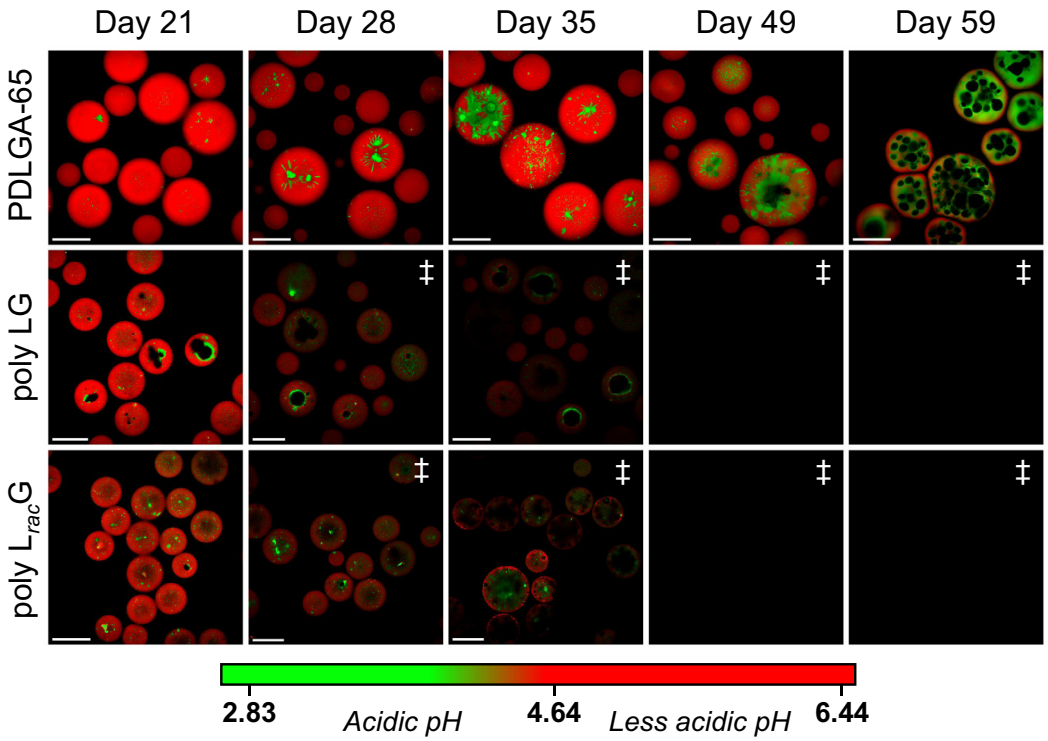

Fig. 4. Two-photon microscopy images of the internal acidic microclimate distribution images within PDLGA-65, poly $L_{rac}G$, and poly LG at later time points; 21, 28, 35, 49, and 59 d. ‡Ratiometric pH probe response was longer discernable from background autofluorescence resulting from dye-leaching. Scale bar = 100 μm.

have previously characterized the thermal behavior, molecular weight loss, erosion and swelling of the copolymers discussed herein, both as microparticles and small solid implants, and have found the results to be consistent and repeatable, these properties were not monitored again in this study [9–11,13].

The internal pH of microspheres during the first two weeks of incubation was within the detectable range of the pH probe, 2.83 < pH < 6.44. Internal pores, which appear as black holes on the micrograph, were present in all particles but were more prevalent in the sequenced PLGAs and **PLLGA-50**. Initially, all samples exhibited minimal acidity with an internal pH > 4.64. It should be noted that even in the initial image of **PLLGA-50,** regions of apparent low pH appear. These artifacts are likely due to refracting crystals [57–59]. Consistent with this assignment is the fact that microparticle controls without the pH-sensitive dye exhibited the same features (Fig. S7). In addition, differential scanning calorimetry thermograms contained melting transitions spanning 75–125 °C (Fig. S2). After 3 d, the internal pH of **PDLGA-50** slightly decreased while the pH of all other samples remained unchanged. With increasing incubation time, localized regions of acidity appeared in **PDLGA-50** and **PLLGA-50** while the pH within **PDLGA-65**, **poly $L_{rac}G$**, and **poly LG** microparticles remained less acidic. The size of the acidic regions within **PDLGA-50** microparticles were larger compared to **PLLGA-50**. Interestingly, the **PDLGA-50** particles exhibited shape irregularities concomitantly with the onset of increasing acidity at 7 d while all other samples retained their original morphology at this time point. After 9 d, the once localized regions of acidity within **PDLGA-50** percolated throughout the microparticles resulting in a widespread decrease in pH, pH ≈ 4.5. Similar behavior was present in **PLLGA-50** microparticles at 11 d. At this time, the internal structure of **PDLGA-50** had significantly changed, large, acid-filled pores had formed and the internal pH became more acidic, pH < 4.5. By contrast, the frequency of acidic μ-pockets within **PDLGA-65**, **poly $L_{rac}G$**, and **poly LG** microparticles was significantly lower. After an additional week of incubation, **PDLGA-50** lost structural integrity and had become an acid-saturated mass with a pH << 4.5. Interesting, **PLLGA-50** microparticles exhibited a similar distribution of acidity to **PDLGA-50** while maintaining structural integrity.

Between 14 and 21 d, the acidity distribution within **PDLGA-65**, **poly $L_{rac}G$**, and **poly LG** microparticles remained relatively constant. At 21 d, the frequency of acidic μ-pockets within **poly $L_{rac}G$** microparticles had increased, whereas **poly LG** accumulated acid only around the periphery of the internal aqueous pores (Fig. 4). The presence of acidic μ-pockets within **PDLGA-65** also increased and acidic μ-channels branching form larger acid filled pores were also observed. By 28 d, dye levels in **poly LG** and **poly $L_{rac}G$** microparticles had decreased to the point that dye signal could not be distinguished from the background auto-fluorescence. Despite the absence of dye, however, gross internal structural changes can be observed at 35 d. At this time, the prevalence of open pores within **poly $L_{rac}G$** increased resulting in microparticle plasticization after 46 d. In contrast, **poly LG** microparticles retained their original internal structural features until approximately 11 weeks after which the particles exhibit brittle failure to give a powder; no prior plasticization is noted (Fig. S8). For **PDLGA-65**, the frequency and size of acidic μ-pockets increased during the next 2 weeks and significant plasticization was observed by 59 d.

3.4. Trends in pH distribution for sequenced and random PLGA microparticles

To visualize more clearly how the overall pH distribution evolves within samples containing a population of particles (n = 8–10), pH distribution curves for PLGA microparticles were constructed using pixel intensity ratios. The frequency of a specific pH was plotted against the internal pH to monitor any changes in the internal pH distribution (Fig. 5). After 3 d of incubation, the internal pH of all samples remained above pH = 4.5, with the

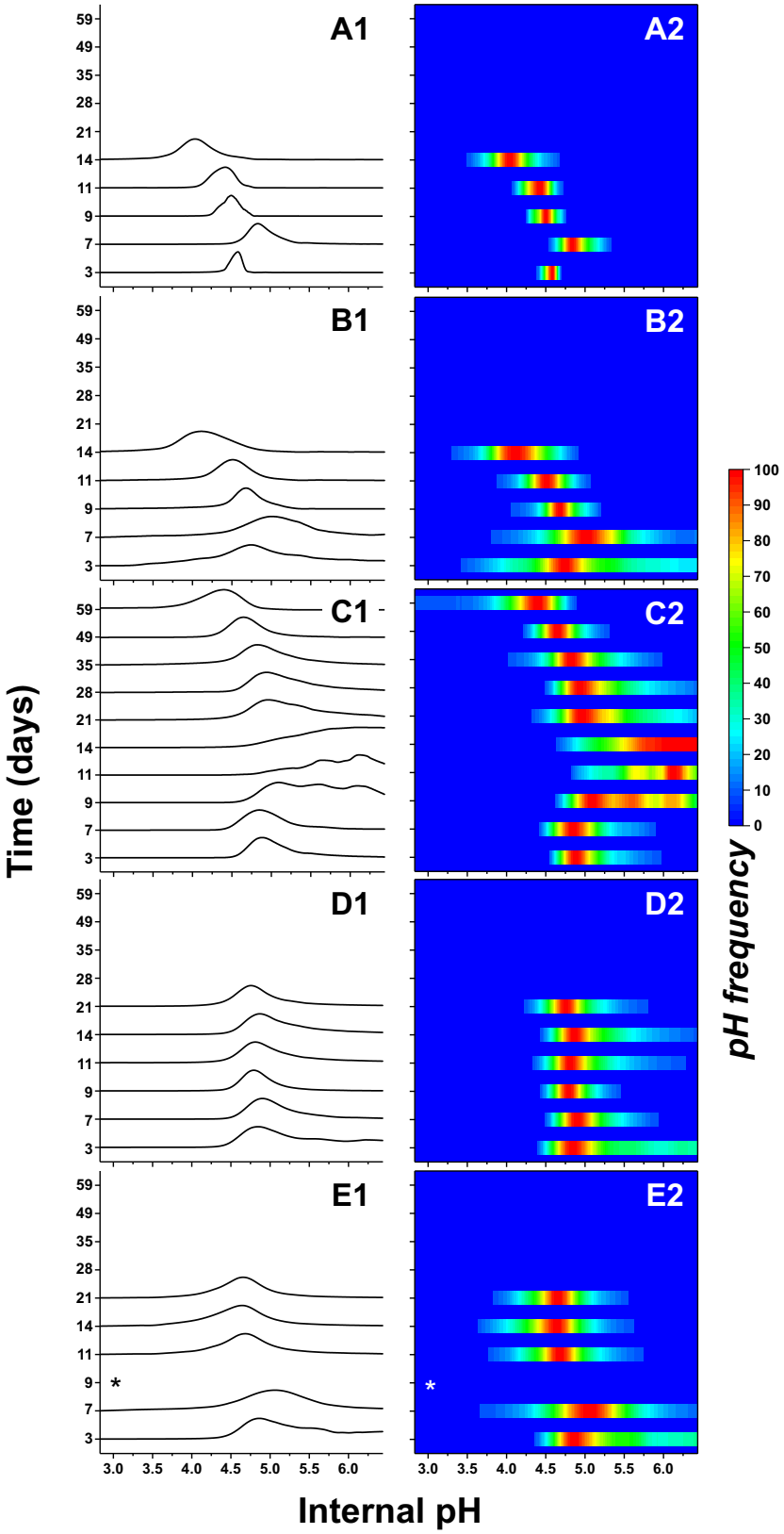

Fig. 5. Internal pH distribution histograms (left) for (A1) PDLGA-50, (B1) PLLGA-50, (C1) PDLGA-65, (D1) poly LG, (E1) poly $L_{rac}G$ microparticles and corresponding pH frequency maps (A2–E2) at specific time points: 3, 7, 9, 11, 14, 21, 28, 35, 49 and 59 days. *Profile not obtained due to laser mode-locking complications. Estimated error in pH ± 0.2 (n = 8–10 microparticles).

distribution varying based on sequence and stereochemistry. **PDLGA-50** had a significantly narrower distribution, pH = 4.5–5.0 compared to all other samples, pH = 4.5–6.0+ . After 7 d, the pH shifts towards a less acidic pH for **PDLGA-50** and **PLLGA-50** while all other samples remained constant. This initial shift in pH for **PDLGA-50** and **PLLGA-50** was immediately followed by a

decreased in pH at 9 d, which continually shifted to a more acidic pH in the following days, 11 and 14. This behavior was also observed in **PDLGA-65** particles but the process was more gradual. The internal pH for **PDLGA-65** particles slowly shifted to a less acidic pH over the second week and then shifted back towards a more acidic pH in the following 5 weeks. Interestingly, the original pH distribution was maintained throughout the course of the experiment for **poly LG** whereas a slight deviation was observed for **poly L_{rac}G**, favoring a more acidic pH.

3.5. External morphology changes in sequenced and random PLGAs

Single-emulsion PLGA microparticle controls (without encapsulated dye) were exposed to physiological conditions over 5 weeks and imaged using SEM to investigate the effects of monomer sequence and stereopurity on microparticle morphology. Representative images of microparticles after 7, 14, 21, 28, and 35 d of incubation are displayed in Fig. 6. After single-emulsion preparation, all microparticles were spherical with non-porous surfaces (Fig. S3). During the first week of incubation, subtle changes in morphology were observed for **PDLGA-50** microparticles. The surface of **PDLGA-50** was slightly textured and small pores had formed on all **PDLGA-50** microparticles. The initial morphology was maintained during this time period for all other samples. Within 14 d of incubation, the external morphology of **PDLGA-50** was severely compromised with evidence of erosion. Large and small pore networks including small channels were observed (Fig. 7A). No changes were observed for the remaining samples until 21 d. At this time, **PDLGA-50** microparticles have lost all structural integrity and have formed plasticized masses. The stereopure random analogue, **PLLGA-50**, no longer retained its spherical shape and changes in surface texture were also observed. In the following week, regions of swelling were observed on the surfaces of **PLLGA-50** microparticles (Fig. 7C), and small pores began to form on the surface of **poly L_{rac}G** microparticles. The morphology of **PDLGA-65** and **poly LG** remained unchanged. After 35 d of incubation, **poly L_{rac}G** microparticles no longer retained their spherical shape and the frequency of small pores had increased with some forming a circular network of pores (Fig. 6D). The regions of swelling remained on the surface of **PLLGA-50** microparticle at this time **PDLGA-65** and **poly LG** remained unchanged (Fig. 6B and E).

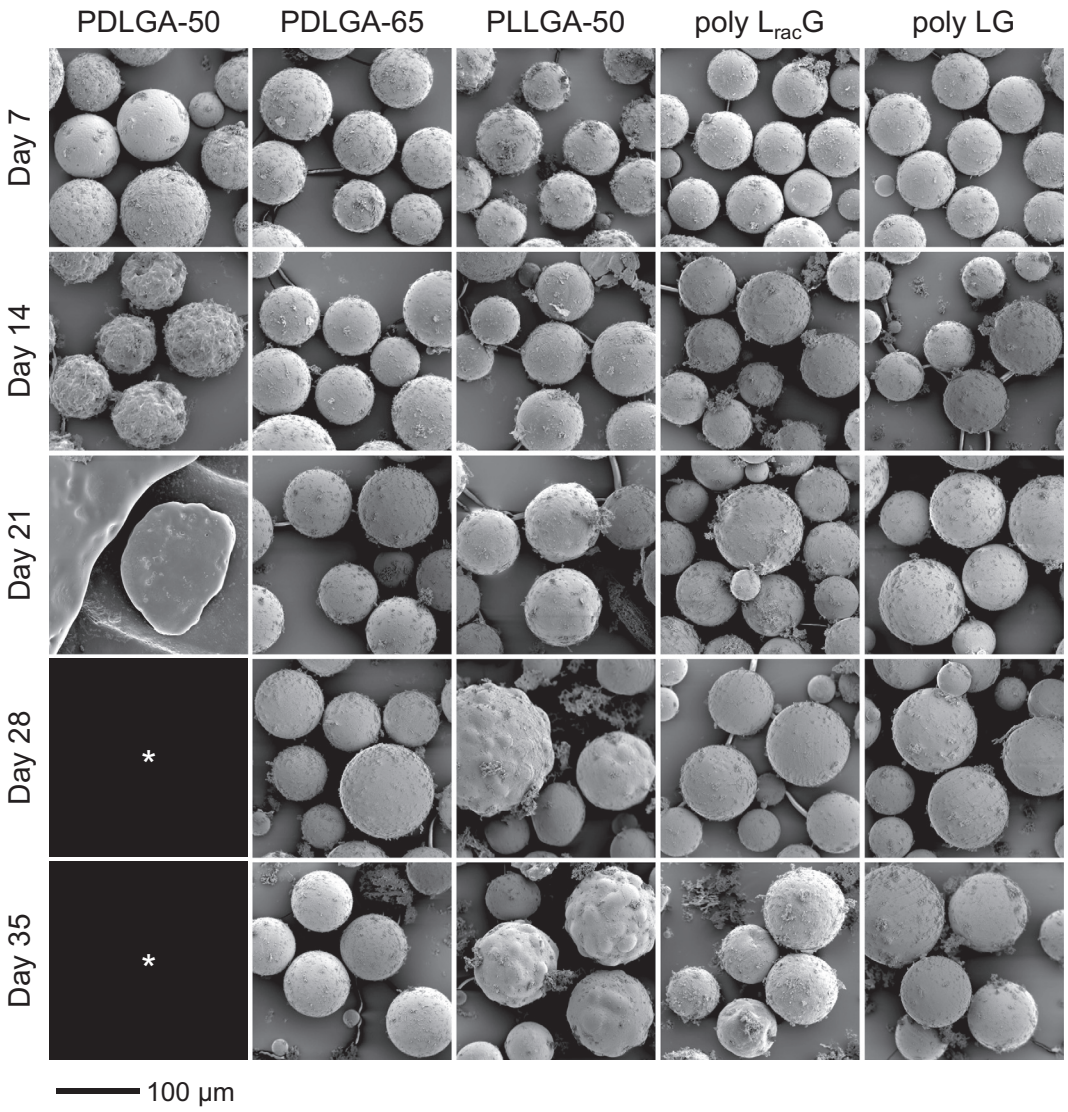

Fig. 6. Scanning electron micrographs of sequenced and random PLGAs after 7, 14, 21, 28, and 35 d *in vitro* under ×350 magnification. *Sample no longer retained structural integrity.

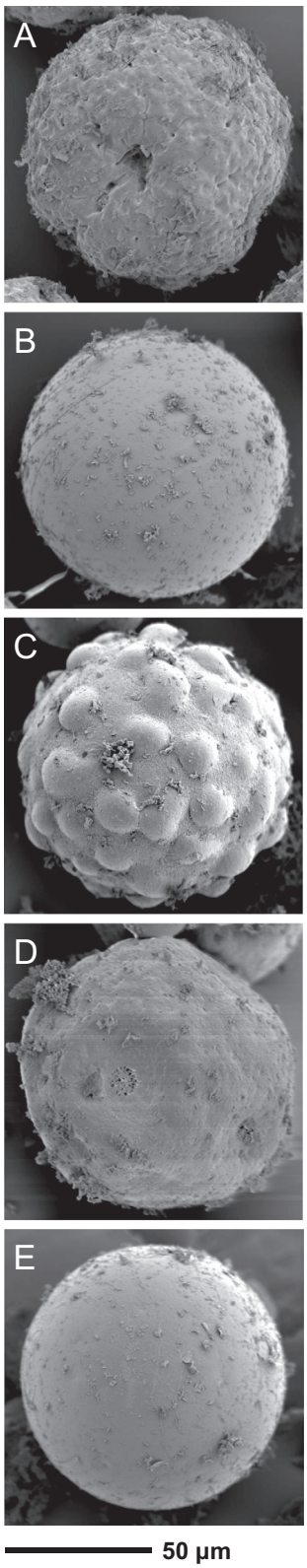

Fig. 7. Scanning electron micrographs of single particles of PDLGA-50 (t = 14 d) (A), PDLGA-65 (t = 35 d) (B), PLLGA-50 (t = 35 d) (C), poly $L_{rac}G$ (t = 35 d) (D), and poly LG (t = 35 d) (E) under ×800 magnification. All images were taken at 35 d with the exception of PDLGA-50, which only retained a spherical morphology up to 14 d.

3.6. Foreign body response to microparticle injections

Microparticles of the sequenced copolymer **poly LG** and the random **PDLGA-50** were subcutaneously injected in mice to monitor the *in vivo* foreign body response at 2 and 4 weeks post-injection (Figs. 8 and S9). These polymers were chosen for comparison because they exhibited a significant difference in acid distribution behavior and degradation profile. The size and morphology of the single-emulsion, blank microparticles were similar as confirmed by SEM (Fig. S10). Histological analysis of subcutaneous depots of both microparticle formulations revealed granulomatous foreign-body reactions. Macrophages and neutrophils were present at 2 weeks post-injection, with somewhat greater neutrophil infiltration in **poly LG** microparticle depots (Fig. S11). By 4 weeks, neutrophils were absent from both particle depots, and foreign-body reactions were characterized by the presence of macrophage foam cells and multinucleated Langhans and Touton giant cells. It is important to note that by week 4, few microparticles of **PDLGA-50** remain and a significant number of multinucleated giant cells can be observed. In contrast, **poly LG** microparticles showed minimal degradation and there were noticeably fewer multinucleated giant cells.

4. Discussion

The current study correlates well with our previous studies on how sequence affects degradation in PLGAs, while providing new insights into the reasons and consequences of those differences. Perhaps the most fundamental finding and one that echoes our prior *in vitro* sequence-based hydrolysis studies in both trends and observed degradation times, is that sequence has a profound influence on the rate of degradation. **PDLGA-50, PLLGA-50**, **poly $L_{rac}G$**, and **poly LG,** which all have the same 1:1 L:G-composition exhibit dramatically different hydrolysis profiles. Indeed, random **PDLGA-50** fails 8 weeks earlier than the alternating stereopure **poly LG**. The alternating sequenced copolymer exhibits a time to failure that more closely resembles that of the random **PDLGA-65**, which has a nearly 2:1 L:G-ratio. This behavior is interesting because many prior studies have correlated degradation times with L:G-ratio and shown that higher L-content translates into slower degradation [7,56,60–66]. It is also clear that stereochemical sequence is important; stereopure versions of both the random and sequenced copolymer degrade more slowly than the racemic copolymers.

As we have discussed in the context of our previous studies, [9–11] the difference in hydrolysis rates between G-G, L-G/G-L, and L-L units is one of the most significant contributors to the range of degradation rates observed (Fig. 9). In random PLGAs, it is well-established that G-rich blocks degrade much more quickly than L-rich blocks. As a result, random PLGAs are rapidly cleaved into shorter chains and the acidic by-products from the cleavage can further accelerate degradation. In contrast, **poly LG** has only two type of linkages, L-G and G-L, both with intermediate and similar cleavage rates. Initial cleavage of the chains is, thus, expected to proceed more slowly and less localization of the cleavage sites and acidic by-products is expected.

The microscopy images acquired in this study increase our understanding of how the molecular level phenomena, including cleavage rates, affect the morphology, acid microclimate distribution, and internal structure. The most prominent change observed in the microparticles as a function of degradation is the shape-distorting plasticization of all the polymers, except **poly LG**. The sequence-based differences in this behavior correlate well with molecular weight loss and the degree of buffer infiltration. With regard to molecular weight, our prior study relating sequence to properties has shown that the rate of molecular weight loss and the degree of swelling and erosion for microparticles and implants prepared from these copolymers exhibits the following trend: **PDLGA-50** > **PLLGA-50** > **poly $L_{rac}G$** > **poly LG** (**PDLGA-65** was not

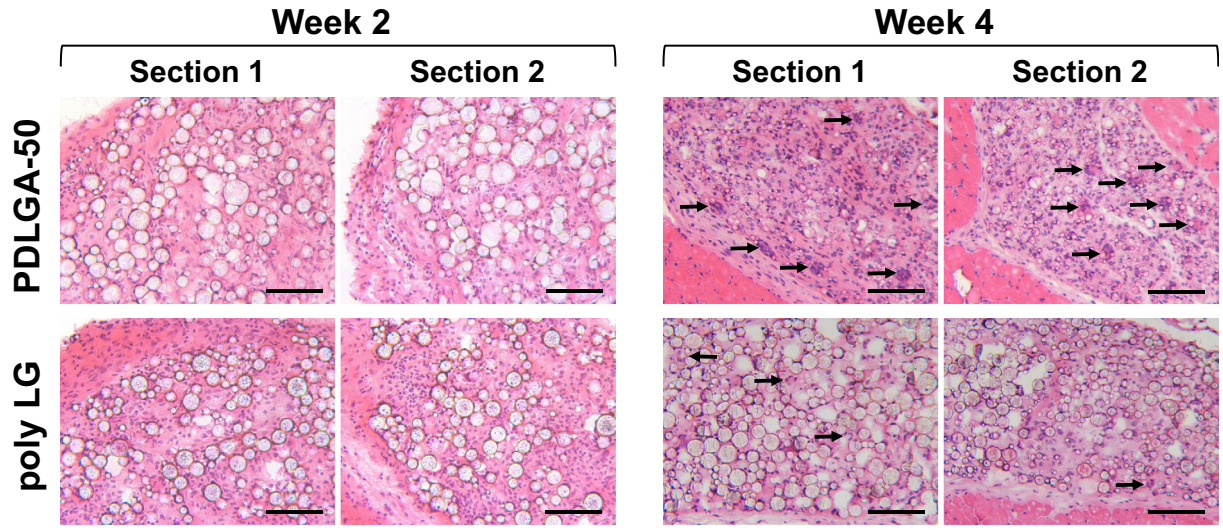

Fig. 8. H&E staining of subcutaneous tissue microparticle depot injections in C57BL/6J wild-type mice, 2 and 4 weeks after injections (×25). Section 1 and 2 are representative sections of tissue from two different mice. Arrows indicate presence of foreign body giant-cells. Scale bar = 100 μm.

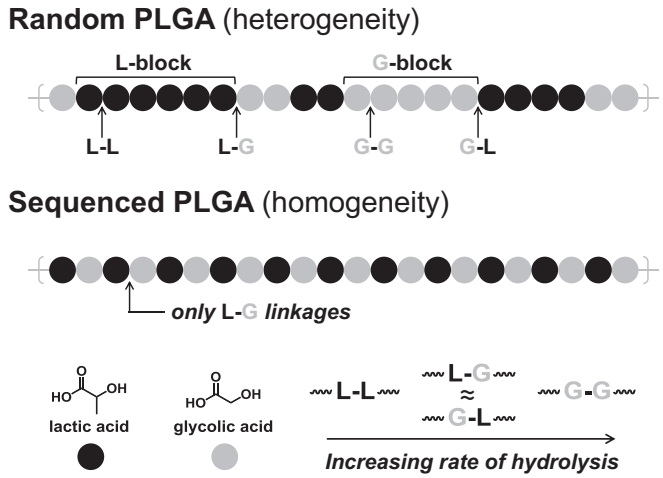

Fig. 9. Linkage type(s) and distribution for PDLGA-50 (top) and poly LG (bottom) with relative linkage hydrolysis rates.

reported in this study but has been characterized relative to PDLGA-50 previously) [7,11,67]. Also, we have seen the plasticization reflected in the broadening and shift of the glass transition temperatures for **PDLGA-50** and **poly $L_{rac}G$** [9].

Buffer infiltration appears to be an important contributor to the observed differences in acid distribution within the particles, especially in the early part of the degradation. The initial shift to higher pH for **PDLGA-50**, **PLLGA-50,** and **PDLGA-65** can be attributed to an infiltration of the buffer and/or clearance of acidic by-products that overwhelms any acid produced by degradation. Consistent with this hypothesis, we found in a prior study that **PDLGA-50** and **PLLGA-50** exhibited a much greater degree of swelling due to buffer infiltration than their sequenced copolymers analogues [11]. Despite the relatively rapid degradation of these random copolymers the large degree of buffer intake is apparently sufficient to neutralize the produced acid. As degradation progresses, however, the acid content builds quickly and there is a shift to a more acidic pH. For **PDLGA-65**, for which swelling is less pronounced, the initial shift to a higher pH is also observed, presumably because the rate of degradation is too slow to overwhelm even a small amount of buffer. It is important to note that early increases in pH for degrading PLGAs, were also reported previously by Schwendeman and coworkers [40]. The sequenced copolymers, **poly LG** and **poly $L_{rac}G$**, do not exhibit this initial shift to higher pH to the same degree as the random analogues. In these cases, the balance between cleavage rate and very minimal swelling, as established by our previous swelling studies, does not result in an early domination of the pH distribution by the buffer.

The initial internal particle structure and dye-loading also differs based on sequence, which we hypothesize may correlate with structural homogeneity of the PLGA copolymers. Immediately after preparation, we observe that sequenced-defined **poly $L_{rac}G$** and **poly LG** microparticles exhibit a higher number of internal voids than the microparticles produced from random PLGAs. Although we did not quantify this parameter, the observation was consistent in all micrographs and for multiple particle preparations. The second observation that the sequenced copolymers would not load as much dye as the random copolymers was obvious in the brightness of the initial images and in the fact that dye levels fell to below observable concentrations for both **poly $L_{rac}G$** and **poly LG** before the particles had failed. In a previous study, we had also noted that we were able to achieve a higher loading of rhodamine-B into **PDLGA-50** vs. **poly LG** microparticles. We suggest that these two observations may be related to the homogeneity of the sequenced copolymers relative to the random analogues. Although we do not observe multiple T_gs for **PDLGA-50,** which would indicate microphase separation, the presence of L- and G-rich blocks must necessarily result in some degree of heterogeneity in the bulk, which will in turn generate areas that have more and less affinity for any solute. The sequenced chains, due to their uniformity must be characterized by a single Flory-Huggins interaction parameter, χ, will likely favor self-interaction and exclude other possible solutes. In the case of particle formation, such self-interaction can lead to the exclusion of the organic solvent used in the preparation of the microparticles. The excluded solvent will coalesce to form droplets, which will lead to the formation of internal voids. Similarly, the homogeneous sequenced copolymers would be expected to exhibit a lower tendency to interact with most solutes, including dyes and drugs, relative to the more heterogeneous random PLGAs. We hypothesize that this phenomenon is responsible for the difficulties that we have experienced in loading such solutes into **poly LG**. The implications of potentially decreased loading relative to the clear benefits in degradation and pH will

need to be investigated further to understand how best to adapt these materials to DDSs.

Our confidence in the sequence-based differences we see using TPM is supported by the similarity of the behavior we observed for the random copolymers to that reported by both Schwendeman and Langer. Specifically, in both reports a shift towards higher pH values was observed after exposure to physiological conditions. This behavior, which was discussed above, was most prominent for random PLGA microparticles with a 50:50 L:G-ratio and less for PLGAs with higher L-content, i.e., 85:15 and 100:0 [30,40,68]. Also, consistent between our studies and others were the reported pH distribution ranges despite the use of different dyes and microscopic techniques. Finally, the morphological changes in the current work were consistent with those reported by Langer and coworkers for **PDLGA-50** microparticles [30].

Finally, we have observed similarities between *in vitro* and *in vivo* microparticle degradation behaviors for sequenced and random PLGAs, which is of particular importance for translation because not all characteristics observed *in vitro* carry over once the material is implanted. First, we see that the differences in degradation time between **PDLGA-50** and **poly LG** are preserved *in vivo*. The **PDLGA-50** microparticles have mostly degraded by the end of 4 weeks of implantation whereas the **poly LG** particles exhibit minimal changes in the same time period. Secondly, the foreign-body response appears to be diminished for the sequenced **poly LG** microparticles. In previous similar studies on random PLGAs, differences in host tissue response have been associated with changes in microparticle surface chemistry and/or local pH due to polymer degradation [69–74]. The TPM studies demonstrated that acid production within the **poly LG** particles is minimal in this time period, thus it seems likely that difference in FBGC response in the current pilot study is primarily due to the variance in degradation rates. Although further investigation will be required to ascertain the *in vivo* response to **poly LG** after longer time periods, the current acidity studies suggest that acid release within the tissue will be more gradual and less likely to provoke an inflammatory response.

5. Conclusions

Microscopic analysis, TPM and SEM, of particles prepared from both random and sequenced PLGAs demonstrates that key *in vitro* and *in vivo* properties related to DDS performance, i.e., degradation rate, accumulation and percolation of acidic by-products, microparticle morphology, and foreign body response can be tuned using precise macromolecular design. These results are consistent with our prior findings that the loss of molecular weight, increase in dispersity, overall swelling, thermal transitions, and erosion during hydrolytic degradation are all a function of LG sequence. In addition, we have confirmed that two-photon microscopy is a viable method for non-invasive monitoring of internal pH that offers advantages relative to CLSM. Future work will focus on improving the loading efficiencies and evaluating the stability and release of acid-sensitive macromolecular payloads for sequence-defined PLGA matrices.

Acknowledgments

The work presented in this manuscript was supported by the National Science Foundation [CHE-1410119]. The authors would like to thank the Center for Biologic Imaging, University of Pittsburgh, specifically Gregory Gibson for his assistance with the two-photon microscopy study and Kevin Alber for data analysis support. Also, thanks to Julio Diaz-Perez for assistance with the histological analysis and to Stephen Weber for helpful discussions.

Appendix A. Supplementary data

Supplementary data associated with this article can be found, in the online version, at https://doi.org/10.1016/j.actbio.2017.10.043.

References

[1] H.K. Makadia, S.J. Siegel, Poly(lactic-*co*-glycolic acid) (PLGA) as biodegradable controlled drug delivery carrier, Polymers 3 (2011) 1377–1397.
[2] F. Danhier, E. Ansorena, J.M. Silva, R. Coco, A. Le Breton, V. Preat, PLGA-based nanoparticles: an overview of biomedical applications, J. Controlled Release 161 (2012) 505–522.
[3] U. Dragan, S. Magdalena, Poly(lactide-*co*-glycolide)-based micro and nanoparticles for the controlled drug delivery of vitamins, Curr. Nanosci. 5 (2009) 1–14.
[4] S.N. Rothstein, S.R. Little, A "tool box" for rational design of degradable controlled release formulations, J. Mater. Chem. 21 (2011) 29–39.
[5] S.N. Rothstein, W.J. Federspiel, S.R. Little, A unified mathematical model for the prediction of controlled release from surface and bulk eroding polymer matrices, Biomaterials 30 (2009) 1657–1664.
[6] S.N. Rothstein, W.J. Federspiel, S.R. Little, A simple model framework for the prediction of controlled release from bulk eroding polymer matrices, J. Mater. Chem. 18 (2008) 1873–1880.
[7] E. Vey, C. Rodger, L. Meehan, J. Booth, M. Claybourn, A.F. Miller, A. Saiani, The impact of chemical composition on the degradation kinetics of poly(lactic-*co*-glycolic) acid copolymers cast films in phosphate buffer solution, Polym. Degrad. Stab. 97 (2012) 358–365.
[8] Y. Wang, Q. Wen, S.H. Choi, FDA's regulatory science program for generic PLA/PLGA-based drug products, Am. Pharm. Rev. (2016).
[9] J. Li, S.N. Rothstein, S.R. Little, H.M. Edenborn, T.Y. Meyer, The effect of monomer order on the hydrolysis of biodegradable poly(lactic-*co*-glycolic acid) repeating sequence copolymers, J. Am. Chem. Soc. 134 (2012) 16352–16359.
[10] J. Li, R.M. Stayshich, T.Y. Meyer, Exploiting sequence to control the hydrolysis behavior of biodegradable PLGA copolymers, J. Am. Chem. Soc. 133 (2011) 6910–6913.
[11] M.A. Washington, D.J. Swiner, K.R. Bell, M.V. Fedorchak, S.R. Little, T.Y. Meyer, The impact of monomer sequence and stereochemistry on the swelling and erosion of biodegradable poly(lactic-*co*-glycolic acid) matrices, Biomaterials 117 (2017) 66–76.
[12] J.F. Lutz, J.M. Lehn, E.W. Meijer, K. Matyjaszewski, From precision polymers to complex materials and systems, Nat. Rev. Mater. 1 (2016) 1–14.
[13] J.F. Lutz, M. Ouchi, M. Sawamoto, T.Y. Meyer, Sequence-controlled polymers: synthesis, self-assembly, and properties, in: ACS symposium series, American Chemical Society, 2014, pp. 408.
[14] J.F. Lutz, M. Ouchi, D.R. Liu, M. Sawamoto, Sequence-controlled polymers, Science 341 (2013).
[15] N. Badi, D. Chan-Seng, J.F. Lutz, Microstructure control: an underestimated parameter in recent polymer design, Macromol. Chem. Phys. 214 (2013) 135–142.
[16] J.P. Cole, A.M. Hanlon, K.J. Rodriguez, E.B. Berda, Protein-like structure and activity in synthetic polymers, J. Polym. Sci., Part A: Polym. Chem. 55 (2017) 191–206.
[17] L. Hartmann, H.G. Börner, Precision polymers: monodisperse, monomer-sequence-defined segments to target future demands of polymers in medicine, Adv. Mater. 21 (2009) 3425–3431.
[18] A.S. Knight, E.Y. Zhou, M.B. Francis, R.N. Zuckermann, Sequence programmable peptoid polymers for diverse materials applications, Adv. Mater. 27 (2015) 5665–5691.
[19] C.K. Qu, J.P. He, Recent developments in the synthesis of sequence controlled polymers, Sci. China-Chem. 58 (2015) 1651–1662.
[20] M.D. Schulz, K.B. Wagener, Precision polymers through ADMET polymerization, Macromol. Chem. Phys. 215 (2014) 1936–1945.
[21] Y. Tabata, H. Abe, Synthesis and properties of alternating copolymers of 3-hydroxybutyrate and lactate units with different stereocompositions, Macromolecules 47 (2014) 7354–7361.
[22] Y. Tabata, H. Abe, Effects of composition and sequential structure on thermal properties for copolymer of 3-hydroxybutyrate and lactate units, Polym. Degrad. Stab. 98 (2013) 1796–1803.
[23] J. Fernández, A. Larrañaga, A. Etxeberria, W. Wang, J.R. Sarasua, A new generation of poly(lactide/epsilon-caprolactone) polymeric biomaterials for application in the medical field, J. Biomed. Mater. Res. Part A 102 (2014) 3573–3584.
[24] J. Fernández, A. Larrañaga, A. Etxeberría, J.R. Sarasua, Effects of chain microstructures and derived crystallization capability on hydrolytic degradation of poly(L-lactide/epsilon-caprolactone) copolymers, Polym. Degrad. Stab. 98 (2013) 481–489.
[25] J. Fernández, A. Etxeberria, J.R. Sarasua, Effects of repeat unit sequence distribution and residual catalyst on thermal degradation of poly(L-lactide/epsilon-caprolactone) statistical copolymers, Polym. Degrad. Stab. 98 (2013) 1293–1299.
[26] J. Fernandez, E. Meaurio, A. Chaos, A. Etxeberria, A. Alonso-Varona, J.R. Sarasua, Synthesis and characterization of poly (L-lactide/epsilon-caprolactone)

statistical copolymers with well resolved chain microstructures, Polymer 54 (2013) 2621–2631.
[27] J. Fernández, A. Etxeberria, J.R. Sarasua, Synthesis, structure and properties of poly(L-lactide-*co*-epsilon-caprolactone) statistical copolymers, J. Mech. Behav. Biomed. Mater. 9 (2012) 100–112.
[28] J. Fernández, A. Etxeberria, J.M. Ugartemendia, S. Petisco, J.R. Sarasua, Effects of chain microstructures on mechanical behavior and aging of a poly(L-lactide-*co*-epsilon-caprolactone) biomedical thermoplastic-elastomer, J. Mech. Behav. Biomed. Mater. 12 (2012) 29–38.
[29] M. Hakkarainen, A. Höglund, K. Odelius, A.C. Albertsson, Tuning the release rate of acidic degradation products through macromolecular design of caprolactone-based copolymers, J. Am. Chem. Soc. 129 (2007) 6308–6312.
[30] K. Fu, D.W. Pack, A.M. Klibanov, R. Langer, Visual evidence of acidic environment within degrading poly(lactic-*co*-glycolic acid) (PLGA) microspheres, Pharm. Res. 17 (2000) 100–106.
[31] M. van de Weert, W.E. Hennink, W. Jiskoot, Protein instability in poly(lactic-*co*-glycolic acid) microparticles, Pharm. Res. 17 (2000) 1159–1167.
[32] S. Xie, Q. Zhu, B. Wang, H. Gu, W. Liu, L. Cui, L. Cen, Y. Cao, Incorporation of tripolyphosphate nanoparticles into fibrous poly(lactide-*co*-glycolide) scaffolds for tissue engineering, Biomaterials 31 (2010) 5100–5109.
[33] B. Gu, Y. Wang, D.J. Burgess, In vitro and in vivo performance of dexamethasone loaded PLGA microspheres prepared using polymer blends, Int. J. Pharm. 496 (2015) 534–540.
[34] B.S. Zolnik, D.J. Burgess, Evaluation of in vivo–in vitro release of dexamethasone from plga microspheres, J. Control. Release 127 (2008) 137–145.
[35] A. Schadlich, S. Kempe, K. Mader, Non-invasive in vivo characterization of microclimate pH inside in situ forming PLGA implants using multispectral fluorescence imaging, J. Controlled Release 179 (2014) 52–62.
[36] F. Eisenächer, A. Schädlich, K. Mäder, Monitoring of internal pH gradients within multi-layer tablets by optical methods and epr imaging, Int. J. Pharm. 417 (2011) 204–215.
[37] A. Brunner, K. Mader, A. Gopferich, pH and osmotic pressure inside biodegradable microspheres during erosion, Pharm. Res. 16 (1999) 847–853.
[38] K. Mäder, B. Gallez, K.J. Liu, H.M. Swartz, Non-invasive in vivo characterization of release processes in biodegradable polymers by low-frequency electron paramagnetic resonance spectroscopy, Biomaterials 17 (1996) 457–461.
[39] Y. Liu, S.P. Schwendeman, Mapping microclimate pH distribution inside protein-encapsulated PLGA microspheres using confocal laser scanning microscopy, Mol. Pharm. 9 (2012) 1342–1350.
[40] A.G. Ding, S.P. Schwendeman, Acidic microclimate pH distribution in PLGA microspheres monitored by confocal laser scanning microscopy, Pharm. Res. 25 (2008) 2041–2052.
[41] L. Li, S.P. Schwendeman, Mapping neutral microclimate pH in PLGA microspheres, J. Controlled Release 101 (2005) 163–173.
[42] J.C. Kang, S.P. Schwendeman, Determination of diffusion coefficient of a small hydrophobic probe in poly(lactide-*co*-glycolide) microparticles by laser scanning confocal microscopy, Macromolecules 36 (2003) 1324–1330.
[43] A. Shenderova, T.G. Burke, S.P. Schwendeman, Evidence for an acidic microclimate in PLGA microspheres, Proc. Controlled Release Soc. (1998) 265–266.
[44] Y. Liu, A.H. Ghassemi, W.E. Hennink, S.P. Schwendeman, The microclimate pH in poly(D, L-lactide-*co*-hydroxymethyl glycolide) microspheres during biodegradation, Biomaterials 33 (2012) 7584–7593.
[45] S.N. Rothstein, K.D. Huber, N. Sluis-Cremer, S.R. Little, In vitro characterization of a sustained-release formulation for enfuvirtide, Antimicrob. Agents Chemother. 58 (2014) 1797–1799.
[46] W. Heidemann, S. Jeschkeit-Schubbert, K. Ruffieux, J.H. Fischer, H. Jung, G. Krueger, E. Wintermantel, K.L. Gerlach, pH-stabilization of predegraded PDLLA by an admixture of water-soluble sodiumhydrogenphosphate—results of an in vitro- and in vivo-study, Biomaterials 23 (2002) 3567–3574.
[47] A. Shenderova, A.G. Ding, S.P. Schwendeman, Potentiometric method for determination of microclimate pH in poly(lactic-*co*-glycolic acid) films, Macromolecules 37 (2004) 10052–10058.
[48] A.G. Ding, A. Shenderova, S.P. Schwendeman, Prediction of microclimate pH in poly(lactic-*co*-glycolic acid) films, J. Am. Chem. Soc. 128 (2006) 5384–5390.
[49] M.F. Bennewitz, S.C. Watkins, P. Sundd, Quantitative intravital two-photon excitation microscopy reveals absence of pulmonary vaso-occlusion in unchallenged sickle cell disease mice, Intravital 3 (2014) e29748.
[50] S.C. Watkins, Claudette St. Croix, Current Protocols Select: Methods and Applications in Microscopy and Imaging, 1st ed., John Wiley & Sons, Inc., Hoboken, New Jersey, 2013.
[51] W. Denk, J.H. Strickler, W.W. Webb, Two-photon laser scanning fluorescence microscopy, Science 248 (1990) 73+.
[52] H.J. Park, C.S. Lim, E.S. Kim, J.H. Han, T.H. Lee, H.J. Chun, B.R. Cho, Measurement of pH values in human tissues by two-photon microscopy, Angew. Chem. Int. Ed. 51 (2012) 2673–2676.
[53] R.M. Stayshich, T.Y. Meyer, New insights into poly(lactic-*co*-glycolic acid) microstructure: using repeating sequence copolymers to decipher complex nmr and thermal behavior, J. Am. Chem. Soc. 132 (2010) 10920–10934.
[54] S. Jhunjhunwala, G. Raimondi, A.W. Thomson, S.R. Little, Delivery of rapamycin to dendritic cells using degradable microparticles, J. Controlled Release 133 (2009) 191–197.
[55] R.M. Weiss, J. Li, H.H. Liu, M.A. Washington, J.A. Giesen, S.M. Grayson, T.Y. Meyer, Determining sequence fidelity in repeating sequence poly(lactic-*co*-glycolic acid)s, Macromolecules (2017) 550–560.
[56] J. Kasperczyk, Microstructural analysis of poly[(L, L-lactide)-*co*-(glycolide)] by ^{1}H and ^{13}C nmr spectroscopy, Polymer 37 (1996) 201–203.
[57] J.H. Lee, S. Lee, Y.S. Gho, I.S. Song, H. Tchah, M.J. Kim, K.H. Kim, Comparison of confocal microscopy and two-photon microscopy in mouse cornea in vivo, Exp. Eye Res. 132 (2015) 101–108.
[58] D. Wanapun, U.S. Kestur, D.J. Kissick, G.J. Simpson, L.S. Taylor, Selective detection and quantitation of organic molecule crystallization by second harmonic generation microscopy, Anal. Chem. 82 (2010) 5425–5432.
[59] R.D. Wampler, D.J. Kissick, C.J. Dehen, E.J. Gualtieri, J.L. Grey, H. Wang, D.H. Thompson, J. Cheng, G.J. Simpson, Selective detection of protein crystals by second harmonic microscopy, J. Am. Chem. Soc. 130 (2008) 14076–14077.
[60] S. Lyu, D. Untereker, Degradability of polymers for implantable biomedical devices, Int. J. Mol. Sci. 10 (2009) 4033–4065.
[61] M. Vert, S. Li, H. Garreau, J. Mauduit, M. Boustta, G. Schwach, R. Engel, J. Coudane, Complexity of the hydrolytic degradation of aliphatic polyesters, Die Angewandte Makromolekulare Chemie 247 (1997) 239–253.
[62] T.G. Park, Degradation of poly(lactic-*co*-glycolic acid) microspheres – effect of copolymer composition, Biomaterials 16 (1995) 1123–1130.
[63] S.K. Saha, H. Tsuji, Hydrolytic degradation of amorphous films of L-lactide copolymers with glycolide and D-lactide, Macromol. Mater. Eng. 291 (2006) 357–368.
[64] S.M. Li, H. Garreau, M. Vert, Structure-property relationships in the case of the degradation of massive poly(α-hydroxy acids) in aqueous media, J. Mater. Sci. Mater. Med. 1 (1990) 131–139.
[65] C. Engineer, J. Parikh, A. Raval, Effect of copolymer ratio on hydrolytic degradation of poly(lactide-*co*-glycolide) from drug eluting coronary stents, Chem. Eng. Res. Des. 89 (2011) 328–334.
[66] H. Keles, A. Naylor, F. Clegg, C. Sammon, Investigation of factors influencing the hydrolytic degradation of single PLGA microparticles, Polym. Degrad. Stab. 119 (2015) 228–241.
[67] E. Vey, C. Rodger, J. Booth, M. Claybourn, A.F. Miller, A. Saiani, Degradation kinetics of poly(lactic-*co*-glycolic) acid block copolymer cast films in phosphate buffer solution as revealed by infrared and raman spectroscopies, Polym. Degrad. Stab. 96 (2011) 1882–1889.
[68] A. Shenderova, T.G. Burke, S.P. Schwendeman, The acidic microclimate in poly (lactide-*co*-glycolide) microspheres stabilizes camptothecins, Pharm. Res. 16 (1999) 241–248.
[69] J.M. Anderson, A. Rodriguez, D.T. Chang, Foreign body reaction to biomaterials, Semin. Immunol. 20 (2008) 86–100.
[70] J.M. Anderson, M.S. Shive, Biodegradation and biocompatibility of PLA and PLGA microspheres, Adv. Drug Delivery Rev. 64 (2012) 72–82.
[71] K.A. Athanasiou, G.G. Niederauer, C.M. Agrawal, Sterilization, toxicity, biocompatibility and clinical applications of polylactic acid/polyglycolic acid copolymers, Biomaterials 17 (1996) 93–102.
[72] J. Zandstra, C. Hiemstra, A.H. Petersen, J. Zuidema, M.M. van Beuge, S. Rodriguez, A.A. Lathuile, G.J. Veldhuis, R. Steendam, R.A. Bank, E.R. Popa, Microsphere size influences the foreign body reaction, Eur. Cells Mater. 28 (2014) 335–347.
[73] T. Hickey, D. Kreutzer, D.J. Burgess, F. Moussy, In vivo evaluation of a dexamethasone/PLGA microsphere system designed to suppress the inflammatory tissue response to implantable medical devices, J. Biomed. Mater. Res. 61 (2002) 180–187.
[74] J.M. Anderson, R. Lanza, J.A. Thomson, R.M. Nerem, Biocompatibility and bioresponse to biomaterials, in: Principles of Regenerative Medicine,, Academic Press, San Diego, 2008, pp. 704–723.